# Analytical Methods

Accepted Manuscript


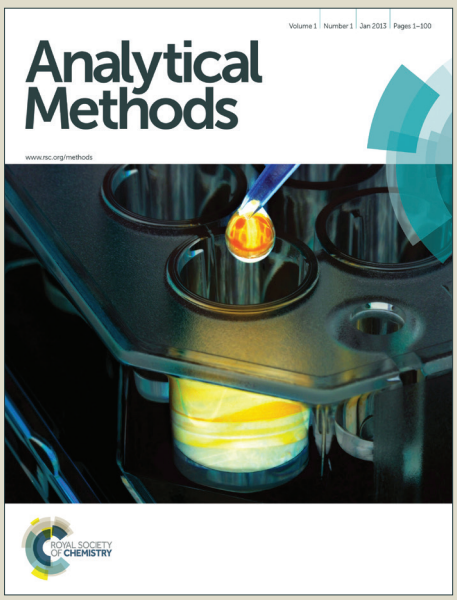



This is an *Accepted Manuscript*, which has been through the Royal Society of Chemistry peer review process and has been accepted for publication.

*Accepted Manuscripts* are published online shortly after acceptance, before technical editing, formatting and proof reading. Using this free service, authors can make their results available to the community, in citable form, before we publish the edited article. We will replace this *Accepted Manuscript* with the edited and formatted *Advance Article* as soon as it is available.

You can find more information about *Accepted Manuscripts* in the Information for Authors.

Please note that technical editing may introduce minor changes to the text and/or graphics, which may alter content. The journal's standard Terms & Conditions and the Ethical guidelines still apply. In no event shall the Royal Society of Chemistry be held responsible for any errors or omissions in this *Accepted Manuscript* or any consequences arising from the use of any information it contains.



ROYAL SOCIETY OF CHEMISTRY

www.rsc.org/methods

# Etching-based transformation of dumbbell-shaped gold nanorods facilitated by hexavalent chromium and their possible application as a plasmonic sensor

Sruthi Ann Alex[a], Jitendra Satija[b], Mohd Azeem Khan[a], Gopalkrishna M. Bhalerao[c], Sujoy Chakravarty[c], Boobalan Kasilingam[d], A. Sivakumar[d], N. Chandrasekaran[a], Amitava Mukherjee[a*]

[a] Centre for Nanobiotechnology, VIT University, Vellore, India.

[b] School of Biosciences and Technology, VIT University, Vellore, India.

[c] UGC-DAE CSR, Kalpakkam Node, Kokilamedu, India.

[d] School of Advanced Sciences, VIT University, Vellore, India.

***Corresponding author**

**Dr. Amitava Mukherjee**

**Senior Professor & Deputy Director**

**Centre for Nanobiotechnology**

**VIT University, Vellore - 632014**

**Email: amit.mookerjea@gmail.com, amitav@vit.ac.in**

**Phone: 91 416 2202620**

**Fax: 91-416-2243092**

Analytical Methods Accepted Manuscript

## ABSTRACT

The seed-mediated synthesis of anisotropic gold nanorods (AuNRs) has attracted attention due to their tunable morphology-dependent optical properties and wide range of applicability. Since the growth of nanorods can be modulated by metal ions, we have explored the Cr(VI)-assisted transformation of AuNRs. In the current investigation, the transformation of dumbbell-shaped AuNRs by Cr(VI) has been studied based on observations from UV–visible spectroscopy, transmission electron microscopy, mean hydrodynamic size measurements, and zeta potential analyses. The Cr(VI)-assisted concentration-dependent reshaping of dumbbell-shaped nanorods to shorter nanorods and spherical particles was observed with a corresponding change in their spectral properties, rod length, and zeta potential. A mechanism to understand this reshaping and etching of dumbbell-shaped nanorods into smooth rods is also proposed. The application of dumbbell-shaped AuNRs for Cr(VI) detection has been presented based on the reshaping effect observed. The method offers a detection limit of 0.071 μM with linearity in the range, 2–10 μM ($R^2$=0.9978). This is the first-ever study, wherein the concentration-dependent transition of dumbbell-shaped AuNRs upon interaction with Cr(VI) was extensively investigated. The method displays good sensitivity and selectivity against most interferents and has been validated in environmental samples (lake, tap, and bore well water) with high recovery rates.


**Keywords:** Gold nanorods; Cr(VI); etching-based transformation; colorimetric detection.

Analytical Methods Accepted Manuscript

## INTRODUCTION

Water pollution by hexavalent chromium ions is of considerable concern as it is more hazardous to public health compared to other valence states of chromium, such as Cr(0) and Cr(III).[1] Due to high mobility and bioavailability, Cr(VI) ions can cause various health problems, including irritation to the respiratory tract, eyes, and skin, and damage of liver and kidney.[2,3] Their prolonged exposure can inevitably result in carcinogenic and mutagenic effects.[4] According to US EPA (United States Environmental Protection Agency) standards, the maximum level of total chromium in drinking water should be 2 μM (100 ppb).[5] Despite stringent government regulations, high influx of Cr(VI) occurs in water majorly from leather tanning industries and, to some extent, from processes like cooling tower water treatment, anti-corrosive plating, wood preservation, and from chromate pigments found in dyes and paints.[6] Therefore, it is highly essential to detect the hexavalent form of chromium in water. Over the years, the estimation of chromium is possible with several analytical techniques, including high-performance liquid chromatography,[7] and inductive-coupled plasma mass spectrometry (ICP-MS),[8] atomic absorption spectroscopy (AAS),[9] and electrochemical method.[10] However, many of these methods are limited by the requirement of sophisticated instruments, field deployability, and cost of analysis.

Advances in nanotechnology have shown some potential developments in Cr(VI) sensing, which are found to be more advantageous over the conventional techniques. Most of these utilize metal nanoparticles (gold and silver metals) as a probe due to their unique surface plasmon resonance (SPR) property and high extinction coefficients ($>10^{-8}$ $M^{-1}cm^{-1}$). These colorimetric sensors are based on the aggregation of metal nanoparticles, and thus, cause a change in the color/absorption intensity/peak wavelength.[11-22] These sensors have offered many advantages, including high



Analytical Methods Accepted Manuscript

sensitivity, rapidity, cost-effectiveness, and no requirement of any sophisticated instrumentation. For example, Tan *et al.* (2011) developed an aggregation-based optical sensor by using 1,4-dithiothreitol-functionalized gold nanoparticles for the selective determination of nanomolar concentrations of Cr(VI) in aqueous solutions.[21] Similarly, Wu *et al.* (2013) used ascorbic acid-capped silver nanoparticles to detect hexavalent chromium ions with 0.050 μM sensitivity.[15] Despite the advantages, universal field deployability of these sensors is sought to be limited due to the large variations in environmental factors, such as temperature, humidity, light, etc., which can accelerate the aggregation of nanoparticles. Also, the presence of interferents in the samples can cause aggregation, and thus this can affect the selectivity of these sensors.

Recently, Li *et al.* (2011) developed a non-aggregation-based highly selective and ultra-sensitive colorimetric sensor for Cr(VI)-detection by using redox etching reaction between gold nanorods (AuNRs) and hexavalent chromium.[22] The rationale behind the selection of AuNRs is their higher extinction coefficients compared to spherical gold nanoparticles and the presence of two plasmon resonance peaks due to their anisotropic structure.[23] The high standard electrode potential of Cr(VI) ions than that of gold atoms led to the oxidative etching of CTAB-capped AuNRs and resulted in large shift in peak wavelength and absorption intensity. The developed method exhibited a detection limit of 0.088 μM, and the sensing method showed a good potential to detect Cr(VI) ions in drinking water and sea water. Although the detection method was demonstrated to have good sensitivity, the mechanism of Cr(VI)-assisted etching of AuNRs was not studied in detail. The sensor response and possible mechanism were based on the spectral observations alone. Few important characterization discussions like variations in morphology, aspect ratio, and surface charge potential of AuNRs were also missing from the report. These



Analytical Methods Accepted Manuscript

characterization studies are essentially required to acquire deeper understanding of the reaction mechanism and might be useful to develop a portable robust field deployable sensor.

Therefore, the present paper focuses on the reaction mechanism of Cr(VI)-mediated etching of AuNRs and their shape-transformation. Unlike the previous study by Li *et al.*, in this paper, we have used dumbbell-shaped AuNRs, which exhibit three surface plasmon peaks. This gives the additional advantage as a detection tool as the disappearance of the third peak occurs even at very low Cr(VI) concentrations. Several characterizations have been carried out to support the mechanism, including TEM imaging, zeta potential measurements, and DLS particle size analysis. To our knowledge, this is the first-ever report to investigate the optical, morphological (shape and aspect ratio), and surface charge modifications observed upon reshaping of dumbbell-shaped AuNRs upon interaction with Cr(VI). Based on the proposed strategy, these dumbbell-shaped AuNRs were applied for the detection of Cr(VI) with a detection limit of 0.071 μM (range: 2–10 μM; $R^2$=0.9978). The strategy offers good sensitivity and selectivity and are comparatively less expensive due to the lower gold concentration and as there is no requirement for any linkers. The practicality of the sensing method was validated in real samples like lake water, tap water, and bore well water with good recovery rates and the method does not require extensive pretreatment.

## 2. MATERIALS AND METHODS

### 2.1. Reagents and solutions

Sodium borohydride ($NaBH_4$), cetyltrimethylammonium bromide (CTAB), and heavy metal salts of $Al^{3+}$, $Hg^{2+}$, $Ni^{2+}$, $Cr^{3+}$, $Cd^{2+}$, $Mg^{2+}$, and $Zn^{2+}$ were purchased from Sigma-Aldrich (India).



Analytical Methods Accepted Manuscript

Hydrogen tetrachloroaurate hydrate ($HAuCl_4.2H_2O$) and heavy metal salt of $Mn^{7+}$, $K_2Cr_2O_7$ (bleaching agent), were procured from SRL Pvt. Ltd. (India). Silver nitrate ($AgNO_3$) was obtained from Merck specialties Pvt. Ltd. (India). Hydrochloric acid (HCl), ascorbic acid, and heavy metal salts of $Fe^{2+}$, $Fe^{3+}$, $Cr^{6+}$, $Co^{2+}$, $Ca^{2+}$, $Cu^{2+}$, $Pb^{2+}$, and $Mn^{2+}$ were bought from SD Fine Chemicals Ltd. (India). All chemicals used in the study were of analytical grade and were used without further purification. Milli-Q water (ultrapure deionized, 18.2 MΩ.cm) from Cascada Bio Water filtration unit (Pall Corporation, Ann Arbor, Michigan, USA) was used for the entire study. Heavy metal stock solutions of 50 mM were prepared with Milli-Q water, and the necessary dilutions were made from these stocks. All glassware was meticulously cleaned using aqua regia ($HCl:HNO_3$ = 3:1) solution, followed by thorough rinsing with Millipore water and drying in a convective hot-air oven.

### 2.2. Synthesis of dumbbell-shaped AuNRs

The dumbbell-shaped AuNRs were prepared by seed-mediated method as described earlier by El-Sayed *et al*., but with some necessary modifications.[24] Concisely, the seed solution was prepared by rapid addition of 0.3 mL of freshly prepared ice-cold $NaBH_4$ solution (0.01 M) to a stirred mixture of 2.5 mL of $HAuCl_4$ (0.5 mM) and 2.5 mL of CTAB (0.2 M). Instantly, the solution turned to light brown color indicating the formation of very tiny gold nanoparticles (or gold seed particles). The resulting colloidal solution was incubated for 3 h at 30°C.

For growth solution preparation, 2.8 mL of ascorbic acid solution (0.079 M) was added to a beaker containing a mixture of gold (III) chloride (100 mL, 0.75 mM), CTAB (100 mL, 0.2 M), and $AgNO_3$ (12 mL, 4 mM) solution. This immediately turned the solution from yellowish orange to a colorless solution due to the reduction of $Au^{3+}$ to $Au^{+}$ by ascorbic acid (mild reducing agent). To this mixture, 12 µL of the as-prepared seed solution was added, followed by a 24-h



Analytical Methods Accepted Manuscript

incubation at 30°C for the completion of the growth of AuNRs. To remove spherical particles (if any) and excess of CTAB from the solution, AuNRs were washed twice by repeating the cycles of centrifugation (9000 rpm for 30 min) and re-dispersion in Millipore water. The purified AuNR solution was stored at room temperature (28°C) till further use.

### 2.3. Interaction of AuNRs and Cr(VI) ions

The interaction between AuNRs and hexavalent chromium was investigated in a concentration-dependent manner. In 2.0-mL eppendorf tubes, colloidal solution of purified dumbbell-shaped AuNRs and solutions of Cr(VI) salt of different concentrations (i.e. 5, 10, 100, 1000 μM) were taken in 2:1 volume ratio. The pH of the solution was adjusted to 1.0 with 1 N HCl as low pH favors the oxidation of the surface gold atoms and thus accelerates the shape conversion process of AuNRs.[25] The resulting colloidal solutions were kept in a dry bath oven at 65°C for 30 min. Thereafter, the tubes were immediately transferred to a cold bath (maintained at 4°C) for rapid cooling of the samples. After 5 min, all the samples were removed and used for characterization after dilution with Millipore water in the volume ratio 1:2.

### 2.4. Cr(VI) detection in real samples

The Cr(VI)-based AuNR etching strategy was adopted to detect Cr(VI) in three different types of practical samples, i.e. lake water, tap water, and bore well water. The lake water samples were obtained from the surface of the VIT University Lake. The tap water samples were collected from the VIT University. The bore well water samples were collected from the locality of Puliyanthangal village, Vellore. The collected samples were filtered first with Whatman filter paper (grade 1, pore size = 11 μm) and then through a membrane filter (pore size = 0.22 μm). All the filtered samples were stored at 4°C and used for study within 24 h of collection.

Analytical Methods Accepted Manuscript

## 2.5. Characterization

All the colloidal solutions were characterized by a UV–visible spectrophotometer (UV-2600, Shimadzu, Tokyo, Japan), in the range of 200–900 nm. For TEM grid preparation, all the samples were first concentrated using centrifugation and then re-dispersion in 100 µL of Millipore water. The homogenous colloidal solutions were sonicated for 10 min and then dropped onto the carbon-coated copper grids and dried. TEM imaging was performed using Philips, CM200, (Netherlands) at 200 kV. The size and aspect ratio (length/breadth) measurements were done from the TEM images using Image-J software. For nanoparticle size and shape distribution, more than 100 particles were measured from the TEM micrograph. Since in few samples, nanorods were of dumbbell-shaped, the average breadth was calculated by taking the mean value of the length at the middle (D1) and both terminals of the nanorods (D2 and D3).

The mean hydrodynamic sizes of nanorods were measured using 90 Plus Particle Analyzer, Brookhaven Instruments Corporation, USA. The zeta potential measurements of AuNRs before and after interaction with different concentrations of Cr(VI) ions were analyzed with Nano Particle Analyzer (SZ100, Horiba Scientific, Japan). For both the measurements, 3.0 mL of each sample was taken in 10-mm disposable cuvettes, and then the analysis was carried out at 25°C. The particle size measurements were carried out at a detection angle of 90°. The Z-average of the distribution was used to report the length of the major axis of AuNRs. Both the particle size and surface charge analyses were performed four times for each sample.

The crystallinity of the samples and presence of chromium were examined by X-Ray diffraction (XRD) analysis (Bruker, D8 Advance X-ray Diffraction spectrophotometer, German). The analysis was carried out at room temperature using CuKα (λ = 1.504Å) as the radiation



Analytical Methods Accepted Manuscript

source, over the angle ranging from 30° to 120° and a scan speed 4°/min. The powdered samples obtained by the centrifugation of the interacted samples following lyophilization were used for analysis. The resultant XRD values obtained were compared with the standard Joint Committee on Powder Diffraction Standards (JCPDS) cards present in the XRD software.

Quantitative analysis of chromium in the real samples was carried out using a graphite flame atomic absorption spectrometer (Analyst400/HGA 900, Perkin Elmer, USA) at a wavelength of 357.9 nm. The analysis was performed at least three times in triplicate, for each sample.

## 3. Results and Discussion

### 3.1 Cr(VI)-based etching of AuNRs

The seed-mediated AuNR synthesis approach yielded dumbbell-shaped AuNRs with an average aspect ratio of 2.26 (nanorod count > 100; length = 60.01 ± 3.59 and breadth = 22.57 ± 2.45) as seen from the TEM image in Figure 1(a)). A negligible percentage (< 4%) of spherical and other shaped nanoparticles were observed as a byproduct. The colloidal solution of dumbbell-shaped AuNRs exhibited absorption peaks at 531 nm and 779 nm, which were due to the excitation of transverse and longitudinal plasmons, respectively (Figure 1(b)). Since the cross-sectional diameter in the middle of the nanorods is smaller than the width at the terminals of the nanorods, a third peak at ~601 nm was observed.[26]

The interaction of AuNRs with various concentrations of Cr(VI) ions caused a substantial change in the solution color from violet to blue and finally pink (refer to the inset of Figure S1 in supplementary information). The longitudinal plasmonic (LSPR) peak was found to be blue-



Analytical Methods Accepted Manuscript

shifted from 779 nm to 729, 640, and 626 nm for 5, 10, and 100 μM Cr(VI) concentration (curves (a) to (d) in Figure 2(A)), respectively. For all the samples, the observed optical response was obtained from the mixture of both rods and spherical particles. The spectral response indicates that the majority of the AuNRs undergo geometrical transformation/reshaping from longer nanorods to shorter nanorods and spherical nanoparticles. Interestingly, at 1000 μM of Cr(VI) ion concentration, a single absorption peak (at 529 nm) with a very small impression of hump (at 603 nm) was observed, suggesting the dominant presence of spherical nanoparticles (curve (e) in Figure 2(A)). Along with the wavelength shift, the absorbance intensity was observed to be decreased as an inverse function of Cr(VI) ion concentration (refer to Figure S1 in supplementary information for UV–visible spectral data without intensity normalization). For 1000 μM Cr(VI) ion concentration, the peak absorbance intensity decreased by ~60% (from 0.513 to 0.204), evidencing the substantial degree of geometric transformation of the parent nanorods.

TEM image analysis of Cr(VI)-treated AuNR samples corroborated the UV–visible spectroscopy data. Figure 2(B) depicts the TEM images of AuNRs samples after treatment with different concentrations of Cr(VI) ions. It is evident from TEM micrographs that even at low concentrations of Cr(VI) ions, the reshaping of nanorods occurred from dumbbell-shape to smooth nanorod structures. A further increase in Cr(VI) ion concentration transformed the longer nanorods into smaller nanorods and eventually into spherical nanoparticles. Hence, with an increase in Cr(VI) ion concentration, the percentage fraction of nanorods in the mixture was found to be decreased, which was compensated with the increased percentage fraction of spherical nanoparticles (Table 1). For 1000 μM Cr(VI) ion concentration, the percentage fraction of nanorods decreased from ~96% to ~36%, while the percentage fraction of spherical gold



Analytical Methods Accepted Manuscript

nanoparticles increased from 4% to 64% for the highest Cr(VI) concentration. Statistics from the TEM images revealed that aspect ratio decreased from 2.66 (untreated) to 1.58 (1000 μM Cr(VI)) (*Note: only nanorods are included for the aspect ratio calculation, while the nanospheres are omitted*). The average length of nanorods reduced from 60.01 ± 3.59 nm (untreated) to 39.10 ± 3.94 nm (treated with 1000 μM Cr(VI)). For the average breadth measurements, the mean value of the length at the middle and both terminals for a minimum of 100 nanoparticles were calculated, and the mean of these values were reported as breadth of the AuNRs. The dumbbell-shaped structures observed in the untreated samples (D1<D2≈D3) were mostly smoothened in the AuNRs treated with 5 μM of Cr (VI), wherein D1 was only slightly lesser than D2 and D3 (D1—central length; D2 and D3—terminal lengths of AuNRs). For higher concentrations of Cr(VI), it can be observed that D1≈D2≈D3, suggesting the complete conversion of dumbbell-shaped AuNRs to smooth nanorods having uniform breadth (refer to Table S1 of supplementary information). The slight increase in the average nanorod diameter with increase in Cr(VI) concentration from 17.90 ± 2.41 nm to 22.57 ± 2.45 nm could be ascribed to the migration of gold from the terminal ends to the side facets of the nanorods. A similar increase in AuNR diameter has been observed earlier during the Cu-assisted reshaping and etching of dog-bone-shaped AuNRs.[25]

The Cr(VI)-mediated reshaping and etching of the nanorods can be explained from the theory of the standard electrode potential (SEP) between gold and chromium. The SEP values for $AuCl_2^-$/Au(0) and $AuBr_2^-$/Au(0) [i.e. SEP of Au(I)/Au(0) in the presence of CTAB ($Br^-$ ions) and HCl ($Cl^-$ ions)] are 1.15 eV and 0.96 eV, respectively, which are lower than the SEP value of Cr(VI)/Cr(III) i.e. 1.33 eV.[27, 28] This difference in SEP causes the reduction of Cr(VI) to Cr(III) on the surface of AuNRs, whereas Au(0) in AuNRs gets etched away by oxidation as $AuCl_2^-$ and



Analytical Methods Accepted Manuscript

$AuBr_2^-$ (redox-based reaction) (Eq. 1 and 2). Since the density of CTAB molecules is very less at the tips compared to the lateral sides of the nanorods,[24] the Cr(VI)-mediated concentration-dependent etching took place preferably from the terminals in the axial direction. In contrast, at the lateral surface of nanorods, the interaction of Cr(VI) ions and AuNRs is diffusion limited due to the presence of compact layer of CTAB and lower surface energy of the facets on the lateral sides of AuNRs.[29] The shape of the nanorods was one of the factors that favored the etching from the terminals. The dumbbell-shaped nanorods have increased curvature at the tips compared to the smooth nanorods, and hence the Au atoms at tips have higher surface energy, which make them more reactive.[25] This is in good agreement with our study as the end-cap smoothening was observed even at low concentrations of Cr(VI). Almost all the nanorods were transformed from dumbbell to smooth nanorods when 5 μM concentration of Cr(VI) ions was used. Further increase in Cr(VI) ion concentration caused a corresponding decrease in the length of the nanorods, which finally transformed into a combination of shorter nanorods and spherical nanoparticles (for 1000 μM). The presence of chromium in the interacted samples was established using XRD analysis of the control AuNRs and AuNRs after treatment with the lowest (5 μM) and highest concentrations (1000 μM) of Cr(VI) (refer to Figure S2 of supplementary information)..

$$8Au^0 + 16Cl^- + 2Cr^{6+} + ½O_2 + 2H^+ \leftrightharpoons 8AuCl_2^- + 2Cr^{3+} + H_2O \qquad \text{Eq. (1)}$$

$$8Au^0 + 16Br^- + 2Cr^{6+} + ½O_2 + 2H^+ \leftrightharpoons 8AuBr_2^- + 2Cr^{3+} + H_2O \qquad \text{Eq. (2)}$$

To further support the Cr(VI)-assisted transformation of AuNRs, dynamic light scattering analysis, and zeta potential measurements were performed. The depolarized dynamic light scattering measurements can be used to determine the length, aspect ratio, and particle size distribution (polydispersity) of rod-shaped nanoparticles. Since DLS is an easier and cheaper



Analytical Methods Accepted Manuscript

alternative to TEM, the size transformation can be tracked using this technique without difficulty, and has the added advantage as no complex calculations are required unlike the indirect estimation of aspect ratio from spectral data..[30,31] DLS analysis revealed a continuous decrease in the length of AuNRs from 72.20 ± 0.35 to 33.58 ± 1.70 nm in the concentration range of 0-1000 μM of Cr(VI) ions. The mean hydrodynamic size analyzed by DLS was slightly higher than the size measured from TEM; however, it is in a proportional correlation with the AuNR length calculated from TEM (Table 1).

The zeta potential measurements also supported the Cr(VI)-assisted geometric transformation of the AuNRs. A progressive decrease in surface charge potential was observed with increasing concentrations of Cr(VI) as indicated in Table 1. For the highest studied concentration of Cr(VI) ion, the zeta potential decreased from +29.33 ± 6.00 to +6.78 ± 1.43. This was attributed to the loss of CTAB molecules on the surface of nanorods due to their size reduction and thereby net decrease in positive charge at their surface.

### 3.2. Detection of Cr(VI) : Potential sensor development

The Cr(VI) concentration-dependent etching of AuNRs was exploited to develop an optical sensor for the selective detection of hexavalent chromium in water. Since the hexavalent form is much more toxic than the trivalent form, the selective sensing of Cr(VI) is highly preferred. In order to attain the maximum sensor response ($\Delta\lambda_{max}$) and lower detection limits, the operation parameters of the method were optimized. The pH (0.7–2.5), temperature (50–75°C), and reagents ratios (volume ratios of AuNRs:Cr(VI)) were tuned to get higher sensitivity (refer to Table S2–S4 of supplementary information). The sensor response was found to be higher for higher temperature and lower pH; however, the stability of the AuNRs at the particular optimization parameter was also taken into account. The sensor response was found to be



Analytical Methods Accepted Manuscript

maximum when the interaction between AuNRs and Cr(VI) ions was carried at pH = 1, temperature = 65°C, and AuNR:Cr(VI) ratio of 1:2 (v/v). After interaction, the signal was found to be stable for more than 1 h (refer to Figure S3 of supplementary information).

Figure 2(A) depicts the effect of Cr(VI) concentration on the plasmonic peak of AuNR colloidal solution. With increase in Cr(VI) ion concentration, ranging from 2 μM to 10 μM, a progressive blue-shift in the LSPR peak wavelength (Figure 4) was observed due to the decrease in aspect ratio of AuNRs. A linear relationship could be established between Cr(VI) concentration and $\Delta\lambda_{max}$ ($R^2 = 0.9978$; inset of Figure 4). The limit of detection of AuNR-based sensor was found to be 0.071 μM (limit of detection = 3 × standard deviation of 5 measurements of blank/slope).[32]

In order to assure the repeatability and accuracy of the system, all the experiments were performed in triplicates. The $p$-value<0.05, calculated from one-way ANOVA, indicated the statistically significant difference between the response obtained for each concentration. Further, run-to-run, day-to-day, and batch-to-batch analyses were carried out for each concentration (in the range of 2 – 10 μM), which indicated the adequately low relative standard deviation (% values) of 1.487, 2.532, and 2.948, respectively (refer to Table S5 of supplementary information). These results ascertain the reproducibility of the method.

To demonstrate the selectivity of the sensor towards Cr(VI) detection, the interaction of AuNRs was investigated with other environmentally relevant heavy metal ions like $Ag^{+}$, $Zn^{2+}$, $Mg^{2+}$, $Mn^{2+}$, $Ni^{2+}$, $Co^{2+}$, $Fe^{2+}$, $Ca^{2+}$, $Pb^{2+}$, $Cd^{2+}$, $Cr^{3+}$, $Mn^{7+}$, $Hg^{2+}$, $Cu^{2+}$, and $Fe^{3+}$. All the interferents, except $Mn^{7+}$, $Hg^{2+}$, $Cu^{2+}$, and $Fe^{3+}$ (at 100 μM ≈ tolerance ratio), were tested at a concentration of 1000 μM, which was 100 times greater than the Cr(VI) concentration (10 μM). Tolerance limit of the system towards interferents was determined based on the maximum concentration of added ions that can cause less than 5% relative error.[33] The sensor response was



Analytical Methods Accepted Manuscript

found to be negligible with most of the interferents (Figure 5). The response to $Mn^{7+}$, $Hg^{2+}$, $Cu^{2+}$, and $Fe^{3+}$ was much lower than the spectral change obtained for Cr(VI), though their concentration was 10 folds higher. The selectivity of a particular system for a definite analyte is based on the particular nanostructure, concentration, and composition of AuNRs present in the solution. Therefore the extent of reshaping and percentage fraction of spherical nanoparticles produced would be much lesser for the other oxidants like $Mn^{7+}$, $Fe^{3+}$ when compared to Cr(VI). In comparison to the existing methods, the present method exhibited better performance as compared to most methods as observed from Table 2, and the current method has the added advantage as it did not involve any complex cross-linking.

### 3.3. Analytical application in real samples

The practical utility and potential applicability of the AuNR-based optical sensor was investigated for the detection of Cr(VI) in environmental water samples like lake water, tap water, and bore well water. Prior to the sensing experiments, the concentrations of total chromium ions (Cr(III)+Cr(VI)) in all types of filtered water samples were determined to be 0.24, 0.68, and 0.8, respectively, using AAS. Thereafter, each of the filtered samples was spiked with three different concentrations of Cr(VI) [4, 6, and 8 μM] and then used for sensing experiments.

The concentrations of Cr(VI) measured by our method are shown in Table 3. The recovery rates for Cr(VI) spiked in lake water, tap water, and bore well water were found to be 97.07–99.58%, 96.66–99.11%, and 96.44–97.88%, respectively. These good recovery percentages indicate that this sensor system can be used as a practical tool for measuring Cr(VI) concentration in natural water samples.

Analytical Methods Accepted Manuscript

## 4. Conclusion

With the help of dumbbell-shaped AuNRs, the role of Cr(VI) ions in sculpturing the AuNRs can be perceived. From the morphology (TEM images) and aspect ratio measurements, the visualization of the etching of dumbbell-shaped AuNRs due to instability at the AuNR tips and their transformation into shorter hemispherical end-capped AuNRs and spherical AuNPs can be understood. The results can be corroborated with spectroscopic, hydrodynamic size and zeta potential analyses. The visualized mechanism was employed for the cost-effective, sensitive (LOD = 0.071 μM; $R^2$=0.9978), and selective detection of Cr(VI) ions using dumbbell-shaped AuNRs as probes. Though the change in end-cap morphology could slightly improve the detection limit, there was a significant reduction in the gold concentration required for the study, which ultimately reduces the cost of analysis. The practicality of the method was substantiated by the Cr(VI) recovery rates in environmental samples like lake water, tap water, and bore well water without requirement for extensive pretreatment. Furthermore, the Cr(VI)-assisted reshaping and etching method can be utilized to tune the dimension and optical properties of the nanorods and for environmental monitoring.

## 5. Acknowledgement

The authors acknowledge the financial support from UGC-DAE Consortium for Scientific Research (UGC-DAE-CSR) for the project (Ref no. CSR-KN/CRS-51/2013-14/650). We gratefully thank VIT University for providing proper lab facilities to carry out the study.

Analytical Methods Accepted Manuscript

## References


1. A. Baran, E. Bıçak, E., Ş. H. Baysal and S. Önal, *Bioresource technology*, 2007, **98**, 661–665.
2. US EPA, Toxicological Review of Hexavalent Chromium, U.S. Government Printing Office: Washington, DC, 1998.
3. S.A. Katz, H. Salem, The Biological and Environmental Chemistry of Chromium, VCH Publishers, New York, 1994.
4. International Agency for Research on Cancer IARC, International Agency for Research on Cancer Monographs on the Evaluation of the Carcinogenic Risks to Humans, vol. 49, Chromium, Nickel, and Welding, IARC Publications, 1990.
5. D. M. Proctor, J. M. Otani, B. L. Finley, D. J. Paustenbach, J. A. Bland, N. Speizer and E. V Sargent, *J. Toxicol. Environ. Heal. Part A*, 2002, **65**, 701–746.
6. C. Pellerin, S. M. Booker and O. F. An, *Environ. Health Perspect.*, 2000, **108**, A402–A407.
7. F. Séby, S. Charles, M. Gagean, H. Garraud and O. F. X. Donard, *J. Anal. At. Spectrom*, 2003, 18, 1386-1390.
8. H. Gürleyük and D. Wallschläger, *J. Anal. At. Spectrom.*, 2001, **16**, 926-930.
9. M. J. Marques, A. Morales-Rubio, A. Salvador and M. De la Guardia, *Talanta*, 2001, **53**, 1229-1239.
10. M. C. Tsai and P. Y. Chen, *Talanta*, 2008, **76**, 533-539.
11. L. Wang, G. Bian, L. Dong, T. Xia, S. Hong and H. Chen, *Spectrochim. Acta Part A*, 2006, **65**, 123–126.
12. L. Zhang, C. Xu and B. Li, *Microchim. Acta*, 2009, **166**, 61–68.
13. C. K. Balavigneswaran, T. S. J. Kumar, R. M. Packiaraj and S. Prakash, *Appl. Nanosci.*, 2014, **4**, 367–378.
14. M. Elavarasi, A. Rajeshwari, S. A. Alex, D. N. Kumar, N. Chandrasekaran and A. Mukherjee, *Anal. Met.*, 2014, **6**, 5161–5167.
15. X. Wu, Y. Xu, Y. Dong, X. Jiang and N. Zhu, *Anal. Met.*, 2013, 5, 560–565.
16. Y. Liu and X. Wang, *Anal. Methods*, 2013, **6**, 1442–1448.
17. M. Elavarasi, S. A. Alex, N. Chandrasekaran and A. Mukherjee, *Anal. Methods*, 2014, **6**, 9554–9560.
18. H. Zhang, Q. Liu, T. Wang, Z. Yun, G. Li, J. Liu and G. Jiang, *Anal. Chim. Acta*, 2013, **770**, 140–146.
19. J. Xin, F. Zhang, Y. Gao, Y. Feng, S. Chen, A. Wu, *Talanta*, 2012, **101**, 122–127.H.
20. L. Zhao, Y. Jin, Z. W. Yan, Y. Y. Liu and H. J. Zhu, *Anal. Chim. Acta*, 2012, **731**, 75–81.
21. F. Tan, X. Liu, X. Quan, J. W. Chen, X. N. Li and H. X. Zhao, *Anal. Methods*, 2011, **3**, 343–347.
22. F.-M. Li, J.-M. Liu, X.-X. Wang, L.-P. Lin, W.-L. Cai, X. Lin, Y.-N. Zeng, Z.-M. Li and S.-Q. Lin, *Sensor Actuat. B Chem.*, 2011, **155**, 817–822.
23. S. Link and M. A. El-sayed, *J. Phys. Chem. B*, 1999, **103**, 8410–8426.
24. B. Nikoobakht and M. A. El-sayed, *Chem. Mater.*, 2003, **15**, 1957–1962.
25. T. Wen, H. Zhang, X. Tang, W. Chu, W. Liu, Y. Ji, Z. Hu, S. Hou, X. Hu and X. Wu, *J. Phys. Chem. C*, 2013, **117**, 25769–25777.
26. S. M. Marinakos, S. Chen and A. Chilkoti, *Anal. Chem.*, 2007, **79**, 5278–5283.


Analytical Methods Accepted Manuscript

27. A. J. Bard, R. Parsons and J. Jordan, Standard potentials in aqueous solution, Marcel Dekker, New York, 1985.
28. D. C. Harris, Quantitative chemical analysis, W. H. Freeman and Company, New York, 7th edn., 2006.
29. Z. L. Wang, *J. Phys. Chem. B*, 2000, **104**, 1153 – 1175.
30. H. Liu, N. Pierre-Pierre and Q. Huo, *Gold Bull.*, 2012, **45**, 187–195.
31. N. G. Khlebtsov, A. G. Mel'nikov, V. A. Bogatyrev, A. V. Alekseeva and B. N. Khlebtsov, *Opt. Spectrosc.*, 2006, **100**, 448–455.
32. V. Thomsen, D. Schatzlein and D. Mercuro, *Spectroscopy*, 2003, **18**, 112–114.
33. M. A. Karimi, H. Abdollahi, H. Karami and F. Banifatemeh, *J. Chin. Chem. Soc.*, 2008, **55**,129-136.

Analytical Methods Accepted Manuscript

## Figure Legend

**Figure 1(a).** TEM image and **(b)** UV–visible spectrum of as-synthesized dumbbell-shaped AuNRs.

**Figure 2(A).** Intensity normalized UV–visible spectral change (blue-shift) of AuNR solution after addition of various concentrations of Cr(VI) [0, 5, 10, 100, and 1000 μM]. **2(B).** TEM image showing the morphology transformation of AuNRs following treatment with different Cr(VI) concentrations [5, 10, 100, and 1000 μM].

**Figure 3.** Schematic representation of Cr(VI) concentration-dependent preferential etching.

**Figure 4.** UV–visible absorption spectra of AuNRs after interaction with different concentrations of Cr(VI) [2–10 μM]. Linear correlation graph with the difference in wavelength ($\Delta\lambda_{max}$) after interaction with the respective concentrations [Figure inset].

**Figure 5.** Comparison of $\Delta\lambda_{max}$ values obtained for AuNRs interacted with 10 μM of $Cr^{6+}$ and higher concentrations of other common interferents [1000 μM of $Ag^{+}$, $Zn^{2+}$, $Mg^{2+}$, $Mn^{2+}$, $Ni^{2+}$, $Co^{2+}$, $Fe^{2+}$, $Ca^{2+}$, $Pb^{2+}$, $Cd^{2+}$, $Al^{3+}$, and $Cr^{3+}$, and 100 μM of $Mn^{7+}$, $Hg^{2+}$, $Cu^{2+}$, and $Fe^{3+}$].

## Table Caption

**Table 1** Particle size and zeta potential analyses from TEM, DLS, and zeta potential analyses.

**Table 2** Comparison of analytical performance of current method for Cr(VI) detection with previous methods.

**Table 3** Estimation of Cr (VI) spiked in different environmental samples.

Analytical Methods Accepted Manuscript

**Table 1** Particle size and zeta potential analyses from TEM, DLS, and zeta potential analyses

| Samples | From TEM | | | | | | Major axis from DLS (nm) | Zeta potential (mV) |
|---|---|---|---|---|---|---|---|---|
| | % spheres[a] | % rod | Length (nm) | Breadth[b] (nm) | Aspect ratio[c] | Spherical Particles Radius (nm) | | |
| AuNR as such | 3.68 | 96.32 | 60.01±3.59 | 22.57±2.45 | 2.66 | 36.42±2.39 | 72.20±0.35 | 29.33±6.00 |
| AuNR +5 µM Cr (VI) | 4.26 | 95.74 | 54.91±2.64 | 22.82±2.06 | 2.41 | 34.46±1.97 | 56.23±0.62 | 21.98±1.96 |
| AuNR +10 µM Cr (VI) | 9.18 | 90.82 | 48.23±2.65 | 23.16±2.03 | 2.08 | 32.41±3.06 | 50.98±1.19 | 19.58±0.55 |
| AuNR +100 µM Cr (VI) | 17.51 | 82.49 | 40.45±3.54 | 23.97±2.08 | 1.69 | 30.88±2.50 | 42.70±1.73 | 12.73±3.02 |
| AuNR +1000 µM Cr (VI) | 63.83 | 36.17 | 39.10±3.94 | 24.69±3.70 | 1.58 | 30.38±4.74 | 33.58±1.70 | 6.78±1.43 |

a – Total count of nanoparticles were greater than 500 for each test concentration.

b – The average breadth measurement is an average of the length at the center and at the two edges of AuNRs.

c – The aspect ratio calculations were based on the nanorods alone. The spherical particles were not taken into consideration for this measurement.



Analytical Methods Accepted Manuscript

**Table 2** Comparison of analytical performance of current method for Cr(VI) detection with previous methods.

| Detection probe | Analyte | Detection method | Mechanism | LOD[#] (µM) | Processing time[#] (min) | Ref. |
|---|---|---|---|---|---|---|
| Dionex-based column set | Cr(III) and Cr(VI) | HPLC - ICP-MS | pH based speciation using anionic and cationic groups in the column | 0.01 | 60 | 7 |
| $^{52}Cr$ and $^{53}Cr$ isotopes | Cr(III) and Cr(VI) | IC-ICPMS | Speciation using anion exchange chromatography | 0.32 | 120 | 8 |
| Activated alumina in polytetrafluoroethylene tube | Cr(III) and Cr(VI) | FAAS | Online retention of Cr(VI) anionic species on alumina microcolumn | 0.84 | 5 | 9 |
| Au-electrodeposited ITO electrodes | Cr(VI) | Electrochemical method | Cyclic voltammetry or hydrodynamic amperometry | 2 | - | 10 |
| Terbium composite nanoparticles | Cr(VI) | Fluorescence | Fluorescence quenching | 0.1 | 5 | 11 |
| Glutathione-capped CdTe quantum dot | Cr(VI) | Fluorescence | Fluorescence quenching | 0.16 | 40 | 12 |
| AgNPs | Cr(VI)<br>Cr(III) and Cr(VI) | UV–visible*<br>UV–visible* | NP aggregation via chelation by Cr(III) | 1.000<br>0.100 | Instant | 13<br>14 |
| Ascorbic acid-capped AgNPs | Cr(VI) | UV–visible* | NP aggregation via chelation by Cr(III) | 0.050 | 10 | 15 |
| Citrate-capped AuNPs | Cr(III) and Cr(VI)<br>Cr(III) and Cr(VI) | UV–visible*<br>Fluorescence* | NP aggregation via chelation by Cr(III)<br>Fluorescence quenching | 0.300<br>0.100 | 45<br>5 | 16<br>17 |
| Glutathione-capped gold nanoclusters | Cr(III) and Cr(VI) | Fluorescence | Fluorescence quenching | 0.050 | 40 | 18 |
| $Ag_{core}$-$Au_{shell}$ NPs | Cr(VI) | UV–visible | Etching of NP shell | 0.010 | 5 | 19 |
| Dithiocarbamate-*N*-benzyl-4-(pyridin-4-ylmethyl)aniline-modified AuNPs | Cr(III) and Cr(VI) | UV–visible* | NP aggregation via chelation by Cr(III) | 0.600 | 60 | 20 |
| Dithiothreitol-capped AuNPs | Cr(VI) | UV–visible | NP aggregation induced by Cr(III) | 0.020 | 10 | 21 |
| AuNRs | Cr(VI) | UV–visible | Etching-based NP transformation | 0.088 | 32 | 22 |
| Dumbbell-shaped AuNRs (aspect ratio : 2.66) | Cr(VI) | UV–visible | Etching-based NP transformation | 0.071 | 35 | Present study |

* Indirect Cr(VI) estimation. Cr(VI) was reduced to Cr(III) and Cr(III) was estimated.

# Detection limit and processing time indicated for Cr(VI) alone.

HPLC: High-performance liquid chromatography; ICP-MS: Inductively coupled plasma mass spectrometry; IC- ion chromatography; FAAS: Flame atomic absorption spectroscopy; ITO: indium-tinoxide; NP: nanoparticle.

Analytical Methods Accepted Manuscript

**Table 3** Estimation of Cr (VI) spiked in different environmental samples.

| Sample source | Cr(VI) concentration from AAS (µM) | Spiked Cr(VI) concentration (µM) | $\Delta\lambda_{max}$ (nm) | Detected concentration (µM) | % Recovery |
|---|---|---|---|---|---|
| Lake water | 0.24 | 4 | 37.02±0.76 | 4.12±0.10 | 97.09±2.42 |
| | | 6 | 72.94±1.10 | 6.21±0.09 | 99.52±1.47 |
| | | 8 | 104.97±0.94 | 8.08±0.06 | 98.02±0.67 |
| Tap water | 0.68 | 4 | 43.88±1.20 | 4.52±0.07 | 96.51±1.50 |
| | | 6 | 78.14±0.76 | 6.51±0.07 | 97.50±1.05 |
| | | 8 | 113.95±0.95 | 8.60±0.06 | 99.08±0.70 |
| Bore well water | 0.8 | 4 | 47.09±0.99 | 4.70±0.08 | 97.99±1.62 |
| | | 6 | 79.00±1.06 | 6.56±0.08 | 96.52±1.11 |
| | | 8 | 112.06±0.45 | 8.49±0.06 | 96.48±0.63 |

Analytical Methods Accepted Manuscript

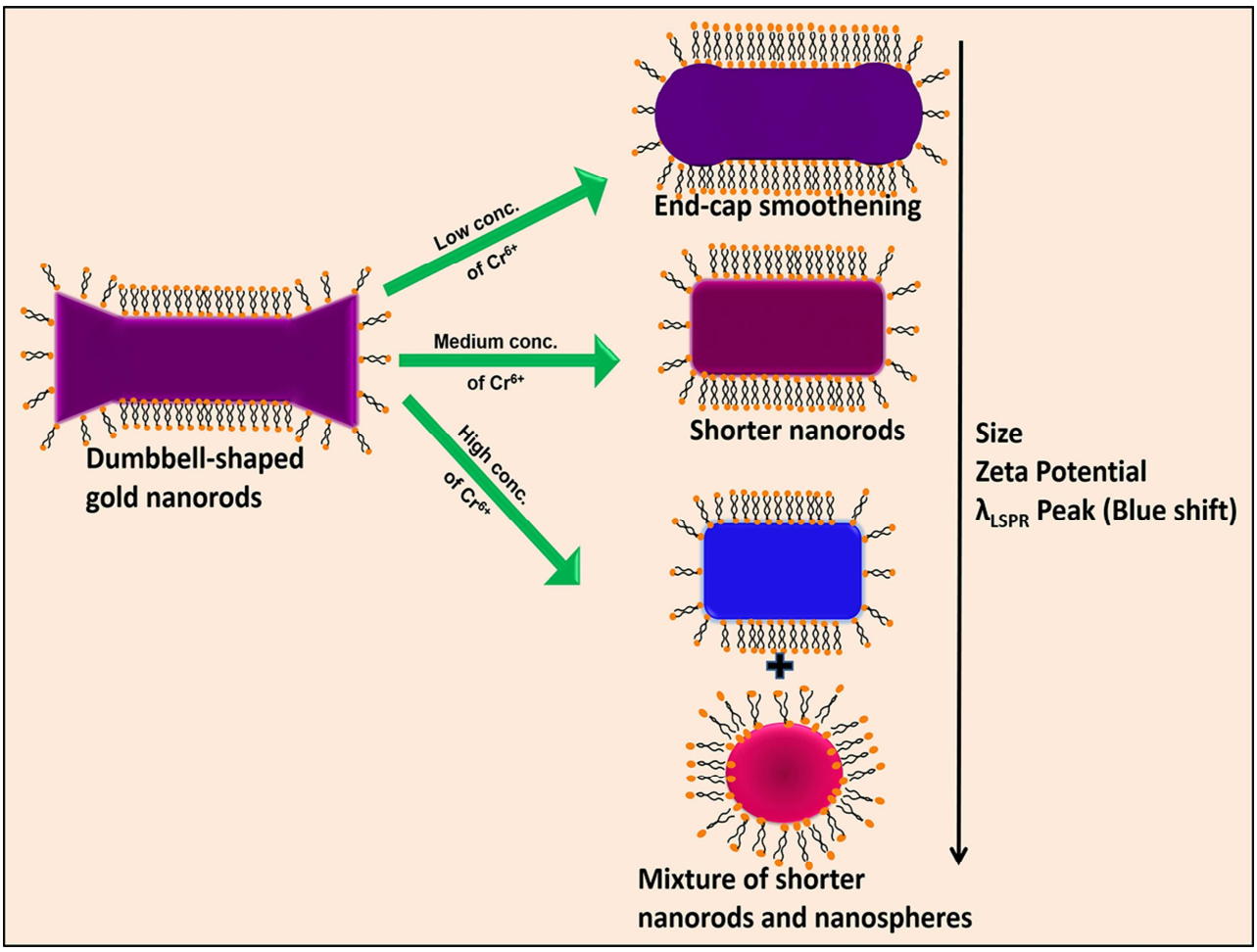


An investigation on the transformation of morphology, aspect ratio, optical properties, and zeta potential of dumbbell-shaped gold nanorods upon interaction with Cr(VI) was performed.

Analytical Methods Accepted Manuscript

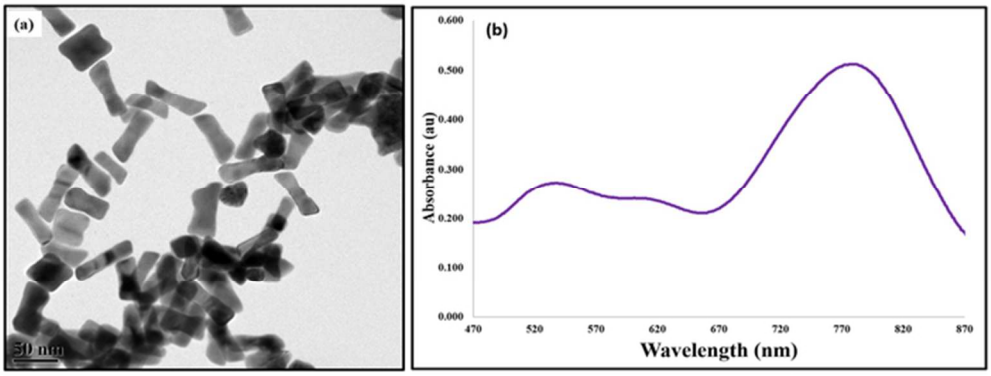


29x11mm (600 x 600 DPI)

Analytical Methods Accepted Manuscript

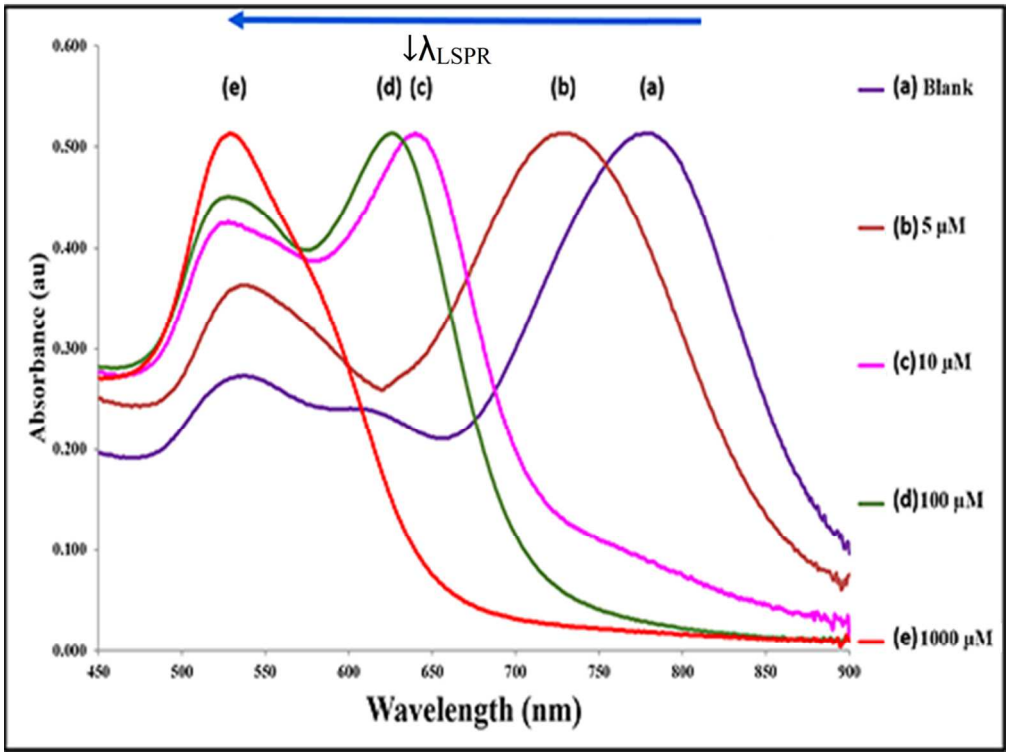


59x45mm (600 x 600 DPI)

Analytical Methods Accepted Manuscript

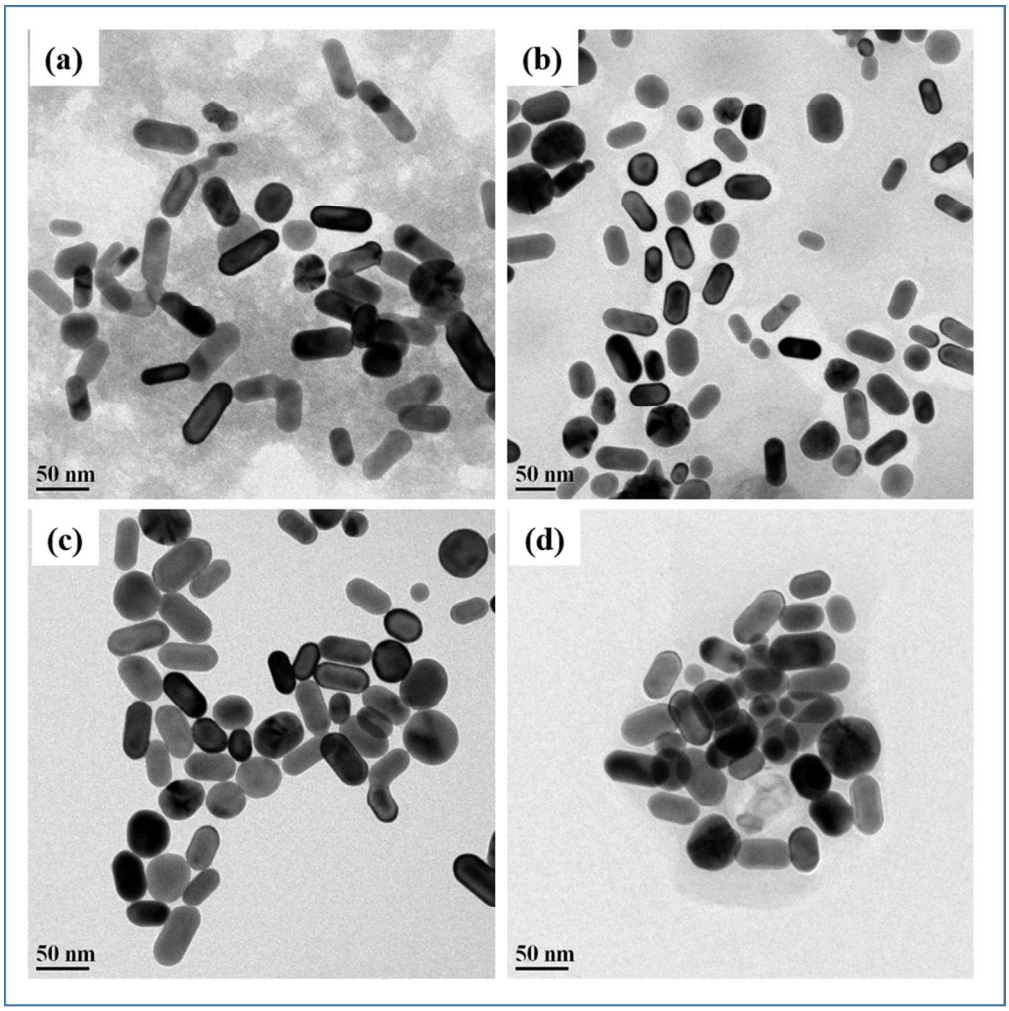


80x80mm (600 x 600 DPI)

Analytical Methods Accepted Manuscript

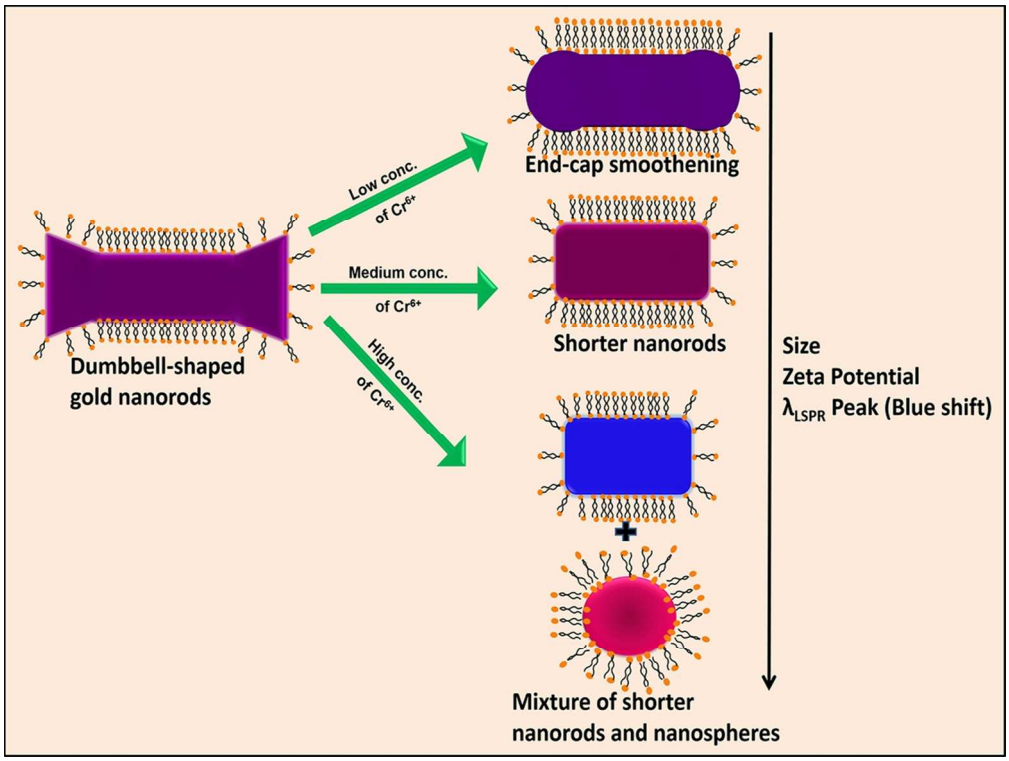


59x45mm (600 x 600 DPI)

Analytical Methods Accepted Manuscript

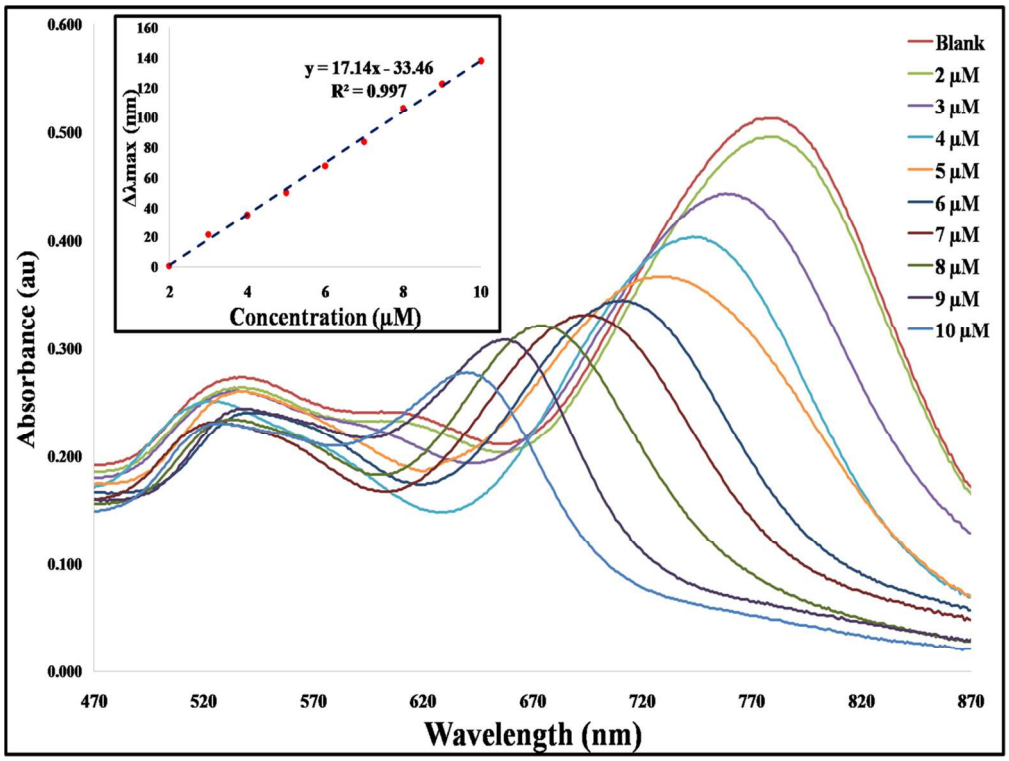


59x45mm (600 x 600 DPI)

Analytical Methods Accepted Manuscript

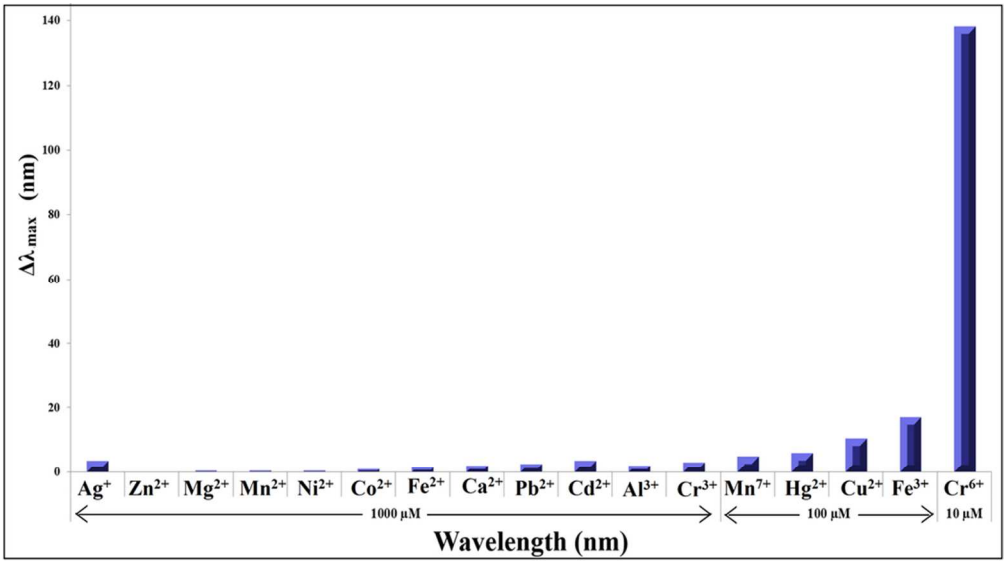


44x24mm (600 x 600 DPI)

Analytical Methods Accepted Manuscript